mathematics

MDPI

Article

New Insights on Robust Control of Tilting Trains with Combined Uncertainty and Performance Constraints

Fazilah Hassan [1,*,†], Argyrios Zolotas [2,*,†] and George Halikias [3,†]

[1] School of Electrical Engineering, Universiti Teknologi Malaysia, Skudai 81300, Johor, Malaysia
[2] Centre for Autonomous and Cyber-Physical Systems, SATM, Cranfield University, Cranfield MK43 0AL, UK
[3] Department of Mathematics, National and Kapodistrian University of Athens, University Campus, 15784 Athens, Greece; ghalikias@math.uoa.gr
* Correspondence: fazilah.hassan@utm.my (F.H); a.zolotas@cranfield.ac.uk (A.Z)
† These authors contributed equally to this work.

Abstract: A rigorous study on optimized robust control is presented for non-preview (nulling-type) high-speed tilting rail vehicles. The scheme utilizes sensors on the vehicle's body, contrary to that of preview tilt (which uses prior rail track information). Tilt with preview is the industrial norm nowadays but is a complex scheme (both in terms of inter-vehicle signal connections and when it comes to straightforward fault detection). Non-preview tilt is simple (as it essentially involves an SISO control structure) and more effective in terms of (the localization of) failure detection. However, the non-preview tilt scheme suffers from performance limitations due to non-minimum-phase zeros in the design model (due to the compound effect of the suspension dynamic interaction and sensor combination used for feedback control) and presents a challenging control design problem. We proposed an optimized robust control design offering a highly improved non-preview tilt performance via a twofold model representation, i.e., (i) using the non-minimum phase design model and (ii) proposing a factorized design model version with the non-minimum phase characteristics treated as uncertainty. The impact of the designed controllers on tilt performance deterministic (curving acceleration response) and stochastic (ride quality) trade-off was methodically investigated. Nonlinear optimization was employed to facilitate fine weight selection given the importance of the ride quality as a bounded constraint in the design process.

Keywords: tilting trains; robust control; optimization; mixed sensitivity; robust performance; active suspensions

MSC: 93D09; 93B36; 93B52; 93C95; 37N35

check for updates

Citation: Hassan, F.; Zolotas, A.; Halikias, G. New Insights on Robust Control of Tilting Trains with Combined Uncertainty and Performance Constraints. *Mathematics* **2022**, *11*, 3057. https://doi.org/10.3390/math11143057

Academic Editors: Mihail Ioan Abrudean and Vlad Muresan

Received: 17 May 2023
Revised: 4 July 2023
Accepted: 7 July 2023
Published: 11 July 2023

Copyright: © 2022 by the authors. Licensee MDPI, Basel, Switzerland. This article is an open access article distributed under the terms and conditions of the Creative Commons Attribution (CC BY) license (https://creativecommons.org/licenses/by/4.0/).

1. Introduction

With the majority of existing high-speed train services in Europe equipped with tilt and growing interest in high-speed trains [1–3], as well as recent developments in metro systems [4], the concept of tilting trains has proven successful and is well established in modern railway vehicle technology.

The tilting principle is relatively simple: on track corners, the vehicle body is typically leaned inward by means of a tilting mechanism in order to reduce passenger lateral acceleration levels. This enables a higher-speed operation through the track corner, and thus a journey time reduction (in fact, the benefit of tilt is greatly seen on railway routes with a high frequency of corners). Advances in control engineering have tremendously benefited active tilting train system technology, with the implementation of active control to achieve the tilt action [5,6].

Early attempts in designing tilting train controllers used what was called the "nulling" tilt control strategy [7], which involves feedback control from a single lateral accelerometer

positioned on the body of the relevant (with reference to needed tilt) passenger vehicle. While the scheme was rather straightforward to implement, trials showed that it was challenging to execute a quick enough response on curve transitions without degrading the ride quality on (straight) track misalignments, as well as system stability.

Today's tilting train services use a command-driven system in which the required tilting angle is ordered by a signal from an accelerometer on a non-tilting part of the preceding vehicle (or front passenger vehicle), with a simple tilt angle feedback controller locally ensuring that each vehicle tilts to the indicated tilt angle [8,9]. This approach, also known as "tilt with precedence", entails using preview tilt data from the vehicle that came before it while applying enough filtering to mitigate the impact of track abnormalities on the tilt command signal. By removing the tilt-information-related sensor from the control-loop, tilt with precedence essentially aims to address the performance difficulties of "nulling"-type techniques. At present, industrial practice acknowledges the preview tilt strategy, although it can be complicated due to the fact that the train must reconfigure when the train direction is changing. It has proven to be challenging to provide the front vehicle with a good performance. It is worth mentioning that GPS systems are occasionally utilized to deliver the "when-to-tilt" (preview) instruction using track database data, although signal quality communication problems, delays, and tunnels may impair the operation and increase complexity [6,7,10]. It should be noted that the control of tilting railway vehicles forms a particular category of railway suspension system control, and other categories exist; for example, the more traditional skyhook-type control in railway vehicles [11], or the more rail-related operational control, i.e., the cruise control of multiple trains [12,13]. This paper strongly contributes to the former category.

A number of previous studies on tilt control do exist in the control literature, i.e., the reader is referred to [6] on active anti-roll bar tilt control, [9] on state-space and estimator-based tilt control, and [14] on multi-objective genetic-algorithm-tuned fuzzy tilt control; however, they do not study robust tilt control. More recently, [15,16] studied the utilization of fractional methods in advanced tilt control design. Robust control design has been a very popular area of research but is mostly followed in non-rail-related domains, with many examples seen in the control literature, i.e., [17–20]. While the work in [21,22] explored H-infinity robust tilt control design, it mainly concentrated on mixed H-infinity/H-2 control and reduced-order H-infinity robust control (neither examined detailed optimization-based robust H-infinity tilt controller design nor ways of utilising the non-minimum phase characteristics of the model in the robust control design). Here, we present a novel yet simple way of designing an optimized robust H_∞ tilt controller (with no preview) via a twofold method: (i) using the non-minimum phase design model and (ii) proposing a factorized design model version with the non-minimum phase characteristics treated as uncertainty (the proposed approach also provides useful insights on the performance level achieved from the various model/uncertainty representations). To the best knowledge of the authors, this is the first time that this approach has been proposed for the non-preview tilt control problem. The tilt control performance trade-off (deterministic vs. stochastic) is appropriately taken in account via the cost function in the optimization and relevant constraints. Both frequency-domain and time-domain (simulation) studies are used to evaluate the controller performance in a rigorous way via detailed simulations.

2. Vehicle Modeling and Design Considerations

The choice of a simple tilting train setup with a single actuation capability, i.e., an active anti-roll bar (ARB) with tilt (roll) actuation only, suffices for the purposes of this work (although there are other tilt mechanisms (see [9]), we emphasize the control design, which can be transferred to other tilt mechanisms). The end-view diagram for such a tilting train setup is shown in Figure 1.

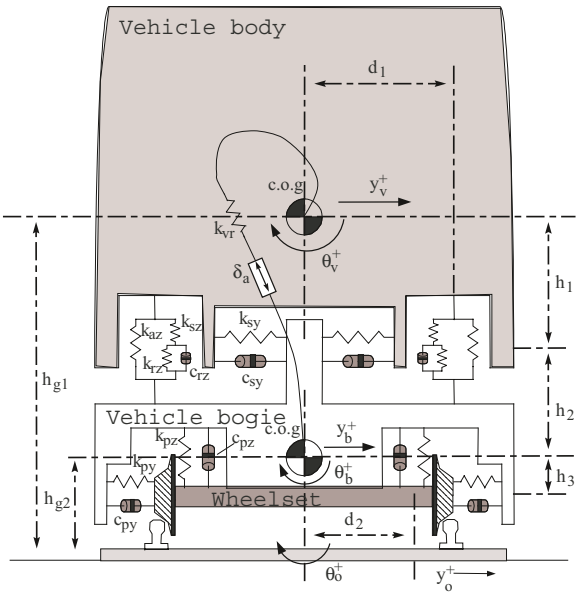

Figure 1. End-view of the tilting vehicle structure.

The modeling of ARB tilting vehicles has been discussed previously in [14,15,21,22], and we employed the mathematical representation presented in [22]. It is worth noting that the dynamic model takes into account the servo-dynamics characteristics of typical tilt actuators (tilt command to applied tilt transfer function). This was included to incorporate a realistic actuator bandwidth capability with parameters chosen to provide a 50% level of damping and a bandwidth of 3.5 Hz (corresponding to a typical dynamic behavior of railway tilt actuator systems).

It is noted that, for analysis and robust control design, the linearized model with an acceptable approximation was used in this paper. In practice, the model will have a form of nonlinearity, depending on what kind of details would be considered, i.e., tilt action from horizon and/or nonlinear actuator dynamics, etc. In terms of the overall roll angle from horizontal (cant + expected tilt), the angle does not exceed 14–16 degrees (due to the link of safety limit for cant elevation and also the allowed tilt angle). The mathematical model used in [22] can be arranged in the usual state-space form.

$$\dot{x}(t) = \mathbf{A}x(t) + \mathbf{B_u}u(t) + \mathbf{B_w}w(t) \tag{1}$$

Note that the state vector, control input, and exogenous input vectors (t) in Equations (2) and (3) are dropped for simplicity.

$$x = \begin{bmatrix} y_v & \theta_v & y_b & \theta_b & \dot{y}_v & \dot{\theta}_v & \dot{y}_b & \dot{\theta}_b & \theta_r & \delta_t & \dot{\delta}_t & y_w & \dot{y}_w \end{bmatrix}^T \tag{2}$$

$$u = [\delta_{ti}], \quad w = \begin{bmatrix} \mathbf{C_{R(1\times2)}} & \mathbf{C_{`0(1\times3)}} & \mathbf{C_{y0(1\times2)}} \end{bmatrix}^T \tag{3}$$

where vectors $\mathbf{C_{R(1\times2)}}, \mathbf{C_{`0(1\times3)}}, \mathbf{C_{y0(1\times2)}}$ include the track curvature, track cant, and track lateral irregularity input components, respectively. Refer to Appendix A for parameters' definitions (as well as their values). As mentioned above, for a more rigorous explanation of the state-space model, the interested reader can refer to [22].

2.1. Track Inputs for the Vehicle

The low-frequency track disturbance (deterministic track input) and the lateral track irregularities (straight track misalignments in the lateral direction referred to as stochastic

track input) are the track excitation (exogenous) inputs. In particular, the stochastic track input velocity spectrum is represented by (4):

$$\dot{S}_{\mathrm{T}}(f_{\mathrm{t}}) = \frac{(2\pi)^2 \Omega_{\mathrm{l}} v^2}{f_{\mathrm{t}}} \qquad (m/s)^2 (Hz)^{-1} \tag{4}$$

where v is the vehicle speed (m/s) and f_{t} is the temporal frequency.

Hence, the lateral track velocity represents a filtered "colored" noise input that rolls off asymptotically at a rate of 20 dB per decade with temporal frequency. For simulation purposes, the lateral track roughness was set at $\Omega_l = 0.33 \cdot 10^{-8}$m, which represents a typically medium-quality rail track structure condition.

The intended geometrical layout of the rail track is where the deterministic track (curved track disturbance) originates. Civil engineers created this to make sure that it will have the desired impact on passenger comfort. Notably, the deterministic track in tilting trains relates to curved sections of the track segments with measurable curvature (R^{-1}, R being the curve radius from a virtual inwards curve centre). In order to minimize the effect of the centrifugal forces felt by the passenger, the track was canted to rotate the vehicle inwards. During the curve transitions, the rates of cant and curvature change linearly but settle on a steady-state curve; refer to Figure 2.

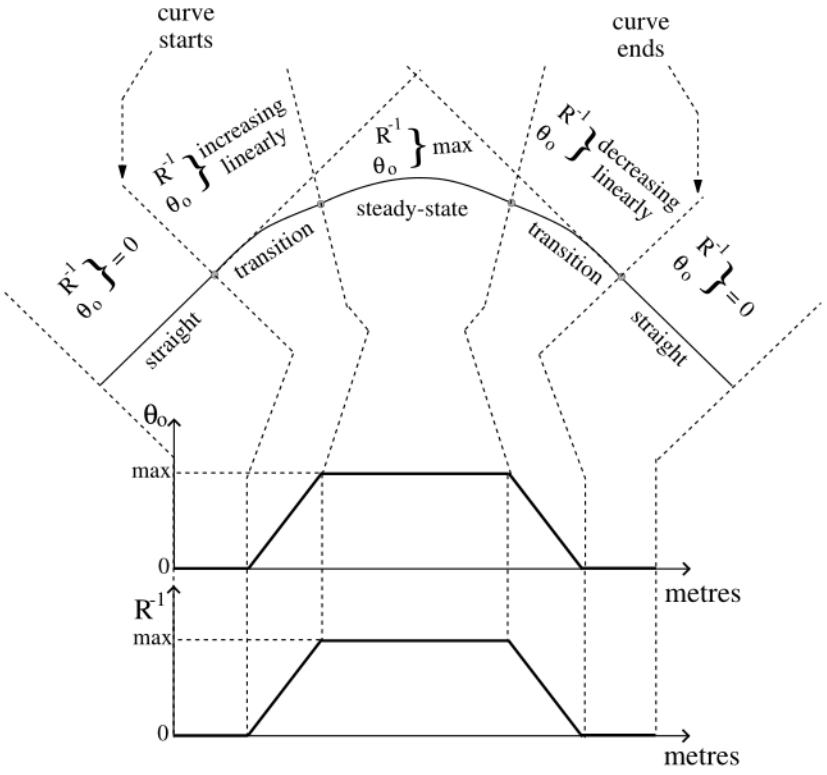

Figure 2. Deterministic track profile representation.

The misalignment dominant spectral characteristics of the lateral track position variable appear at a higher frequency compared to the deterministic input characteristics (but not high enough to be considered completely decoupled). Additionally, the ideal tilt action command is provided by the control input (processed via the actuator servo). For more details, the reader is referred to [9,23].

For simulation and assessment purposes, the track profiles with 60% tilt compensation for curved and straight track irregularities can be found in Table 1.

Table 1. The track test profiles used for simulation and assessment.

Tilt Compensation		60%	Units
deterministic (curved track)			
maximum cant angle	$\theta_{o_{\{\max\}}}$	6.00	(degrees)
maximum curve radius	$R_{\max}$	1000.00	(m)
transition length		145.00	(m) @ each end
track length		1200.00	(m)
stochastic (straight track)			
track roughness	Ω_l	0.33×10^{-8}	(m)
track spatial spectrum	S_T	Ω_l / f^3	$\left(\frac{\mathrm{m}^2}{(\mathrm{cycle/m})}\right)$
track length		1200.00	(m)

2.2. Non-Minimum Phase System Arising from Non-Preview Tilt

Early tilt control design tried to satisfy the full passenger lateral acceleration on a curved track, which proved unsuccessful from a passenger motion sickness perspective [8,23]. Hence, only a portion of tilt was compensated for and the solution was labeled "partial-tilt compensation". This partial-tilt scheme compensation within 60–75% (of lateral acceleration on a steady curve) is provided by the measured acceleration signal and vehicle body roll angle (tilt). This scheme feedback control setup is presented in Figure 3.

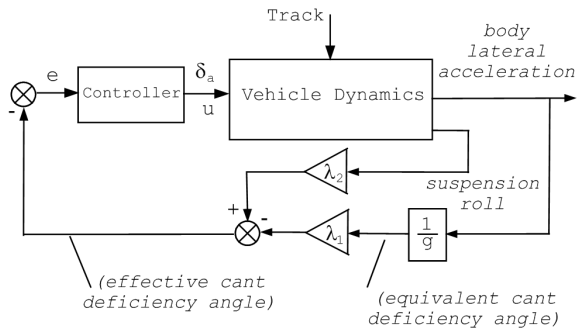

Figure 3. Partial nulling tilt compensation control feedback setup.

The output signal used for feedback control is the so-called effective cant deficiency (which forces the partial-tilt compensation) given by

$$\theta'_{dm} = \left(-\lambda_1 \frac{\ddot{y}_{\mathrm{vm}}}{g} + \lambda_2 \theta_{2sr} \right) \tag{5}$$

where $\ddot{y}_{\mathrm{vm}}$ is the passengers' perceived lateral acceleration, as determined by an accelerometer on the body c.o.g (6), and θ_{2sr} is the secondary suspension roll angle (7).

$$\ddot{y}_{\mathrm{vm}} = \frac{v^2}{R} - g(\theta_o + \theta_{\mathrm{v}}) + \ddot{y}_{\mathrm{v}} \tag{6}$$

$$\theta_{2sr} = \theta_{\mathrm{v}} - \theta_b \tag{7}$$

The parameters λ_1, λ_2 in this work were selected to provide 60% tilt compensation on a steady-state curve (i.e., $\lambda_1 = 0.6, \lambda_2 = 0.4$, respectively, if bogie roll-out is neglected). Note that, in practice, due to the stiff primary suspensions, the bogie roll-out only has a limited effect and can be safely neglected for control design purposes.

From a control-theoretic point of view, the scheme represents a typical single-input–single-output (SISO) structure. The design (nominal) model transfer function is given

by (8). The full mathematical modeling of this transfer function representative can be found in [22].

The nominal model transfer function in (8) represents the dynamic relationship between the output $Y_{(e.c.d)}$ and the control input $\Delta_{(t-i)}$.

Where $Y_{(e.c.d)}$ is the 60% compensation effective cant deficiency and $\Delta_{(t-i)}$ is the ideal control tilt angle.

$$\frac{Y_{ecd}(s)}{\Delta_{t-i}(s)} = \frac{N_t(s)}{D_t(s)} \tag{8}$$

The numerator of the transfer function is given by

$$N_t(s) = 27531(s - 29.36)(s - 6.02)(s^2 + 66.91s + 1066)(s^2 + 7.65s + 24.44) \tag{9}$$

and the denominator

$$\begin{aligned} D_t(s) = (s + 23.2)(s^2 + 1.38s + 17.44)(s^2 + 5.11s + 88) \ldots \\ \ldots (s^2 + 22s + 483.6)(s^2 + 29.15s + 4.9e3) \ldots \\ \ldots (s^2 + 4.83s + 15.9e3)(s^2 + 41.73s + 28.4e3) \end{aligned} \tag{10}$$

The above transfer function refers to the nominal model.

An important point is that the non-preview tilt approach suffers from control bandwidth constraints due to the existence of non-minimum phase (NMP) zeros in numerator $N_t(s)$. These arise due to the location of the suspensions (and the suspension interactions), relative to the centre of gravity and the center of tilt, and the roll angle contribution (from a portion of the gravitational force) measured by the lateral accelerometer. More details on the exact nature of such NMP zeros can be found in [16] and other applications in [24,25].

2.3. Parametric Uncertainty Information

Prior to discussing the approach of setting up the design models for control, we present realistic uncertainty of the vehicle parameters. Four plant perturbations (in addition to the nominal model) were chosen. Table 2 presents the uncertainty details (the variation is relative the nominal model); note that the nominal model is denoted as 'P0'.

Table 2. Perturbed (uncertainty) plant cases.

Plant ID	Perturbation
P1	20% body mass increase
P2	20% body mass decrease
P3	20% decrease in dynamic body mass and 40% (20%) decrease (increase) in secondary suspension damping (stiffness)
P4	20% increase in dynamic body mass and 30% (20%) decrease (increase) in secondary suspension stiffness (damping)

2.4. Design Models for Control

Three alternative plant families are proposed here regarding the modeling for control. As mentioned earlier in the vehicle modeling, the nominal transfer function $G_p(s)= N_t(s)/D_t(s)$ includes a pair of NMP zeros. We present the three representations in a rather developmental way, useful for enabling a better understanding of the level of robust control design in the sequence.

$$\mathbf{\Pi_i}: \quad G_{pp}(s) = G_p(s)(1 + W_i(s)\Delta_i(s)) \tag{11}$$

$$\mathbf{G_p}: \quad G_p(s) = G_{mp}(s)(1 + W_\Delta^{uz}(s)\Delta^{uz}(s)) \tag{12}$$

$$\mathbf{\bar{\Pi}_i}: \quad \bar{G}_{pp}(s) = G_{mp}(s)(1 + \bar{W}_i(s)\bar{\Delta}_i(s)) \tag{13}$$

The first representation, i.e., $\mathbf{\Pi_i}$, comprises the parametric uncertainty in the form of multiplicative uncertainty (the nominal model is the one that includes the NMP zeros). The second representation $\mathbf{G_p}$ presents a factorized model form whereby the NMP zeros are mapped into equivalent multiplicative uncertainty (the virtual nominal plant here includes only the minimum-phase portion, i.e., labeled $G_{\mathrm{mp}}(s)$). The frequency response for both models are illustrated in Figure 4. The third representation $\mathbf{\bar{\Pi}_i}$ presents a factorized model whereby both the parametric uncertainty and the NMP zeros are included in a bulk multiplicative uncertainty form (again, the virtual nominal plant here includes only the minimum-phase portion, i.e., labeled $G_{\mathrm{mp}}(s)$). The reason for proposing the above representations is rather straightforward and essentially addresses the way that the choice of the uncertainty formulation impacts robust control design in the non-preview tilt (in fact, the multiplicative uncertainty weight enters robust stability considerations). In this context, note that $\mathbf{\Pi_i}$ is the normal representation that a designer would employ in a robust H-infinity mixed sensitivity design, and $\mathbf{G_p}$ facilitates exploring whether the conservativeness of mapping NMP zeros into multiplicative uncertainty provides a good enough solution (without considering further uncertainty in the first instance). $\mathbf{\bar{\Pi}_i}$ represents the most conservative representation (with the overall bulk uncertainty form).

Here, we looked into the way to factorize the nominal model into a minimum phase (MP where no non-minimum-phase zeros are included) and the non-minimum-phase zeros as multiplicative uncertainty bound. The feedback setup for this multiplicative uncertainty model can be seen in Figure 5a–c.

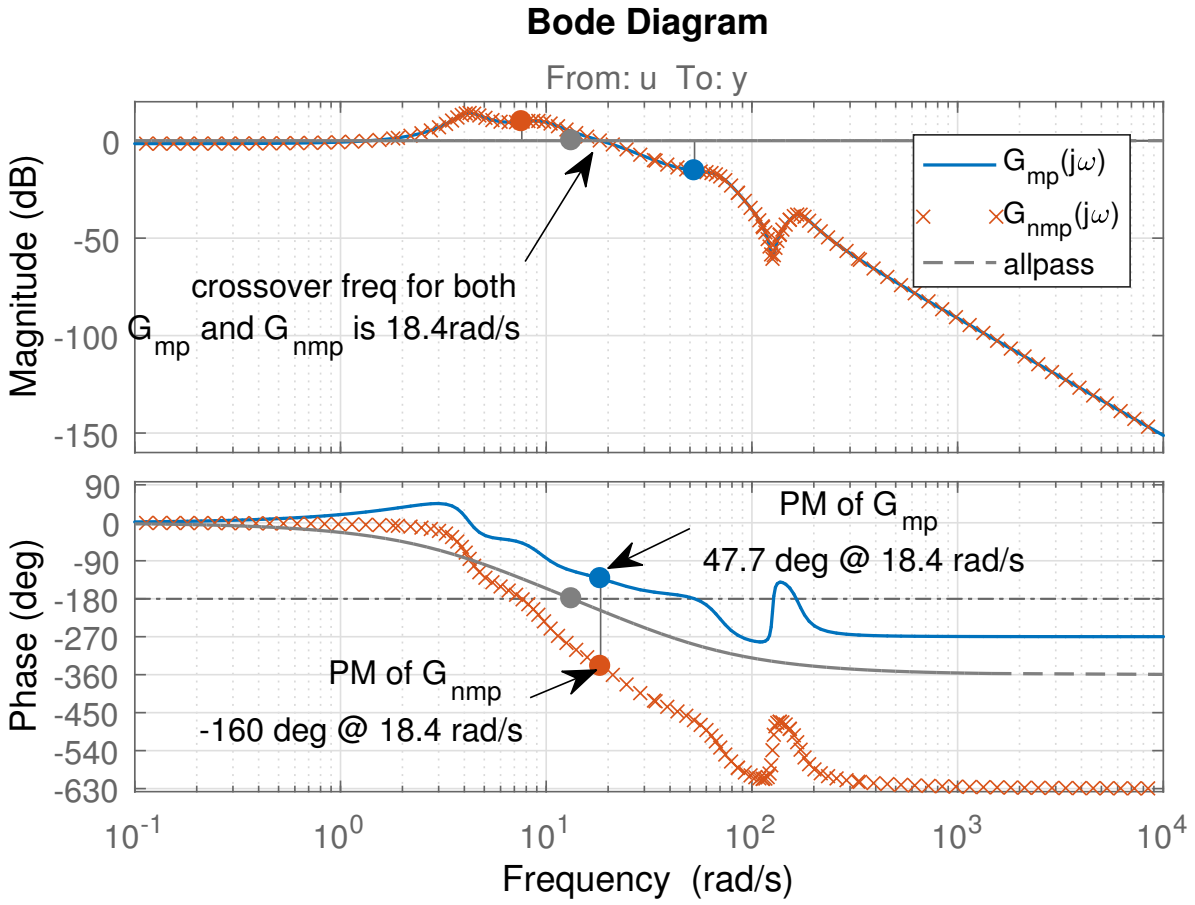

Figure 4. Frequency response of NMP original and of MP factorized TFs.

The transfer function plant $G(s)$ in Equation (12) can be rearranged as

$$G(s) = G_{mp}(s)G_{allp}(s) \tag{14}$$

$G_{allp}(s)$ is an all-pass transfer function (comprising the NMP zeros) and can be expressed in the form of multiplicative uncertainty, as in (12), directly.

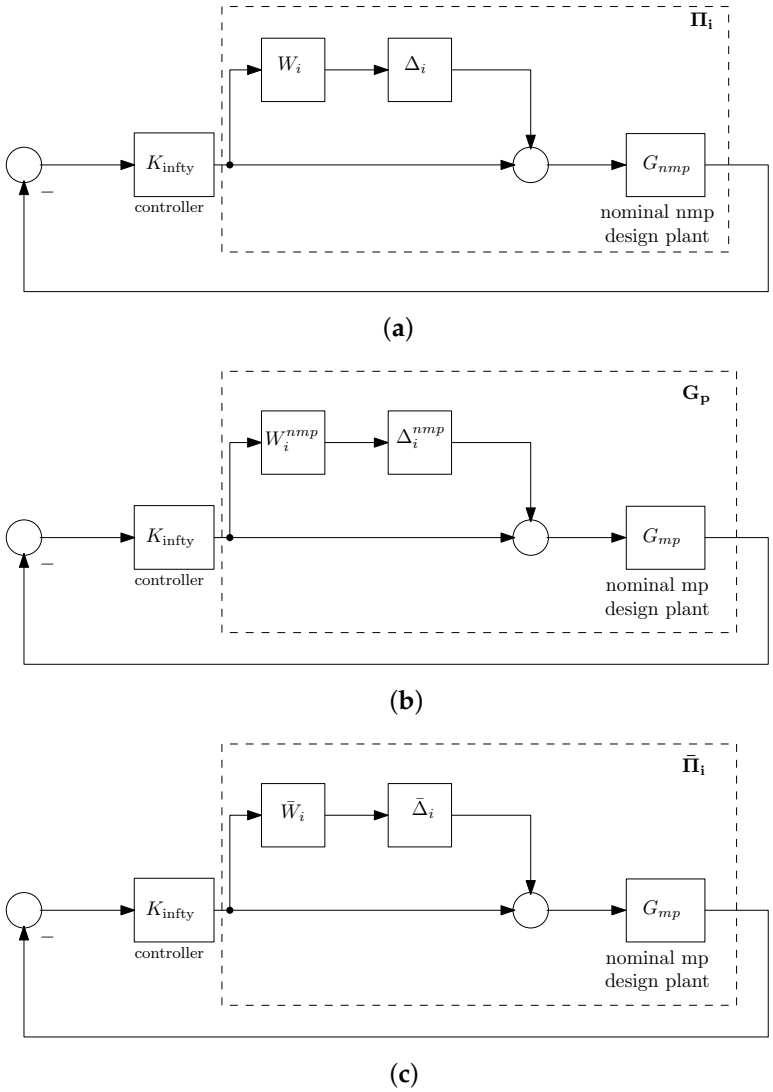

Figure 5. Feedback setup with multiplicative uncertainty. (**a**) The plant family $\mathbf{\Pi_i}$ for the NMP system model. (**b**) The factorized nominal NMP model. (**c**) The overall uncertainty control feedback setup for nominal minimum phase (MP) model.

Recall that Δ(s) is any stable transfer function where $\Delta(j\omega) \leq 1$.

$$W_\Delta(j\omega) = \frac{-j70.76\omega}{(176.7 - \omega^2) + j35.38\omega} \tag{15}$$

The magnitude plot of this particular case of multiplicative uncertainty bound covers the NMP zeros of the system and is presented in Figure 6.

The design approach introduces some conservativeness by representing the NMP zeros as multiplicative uncertainty (nominal), $G_{mp}(s)$.

Note that the two NMP zero frequencies' bandpasses are where the uncertainty is located.

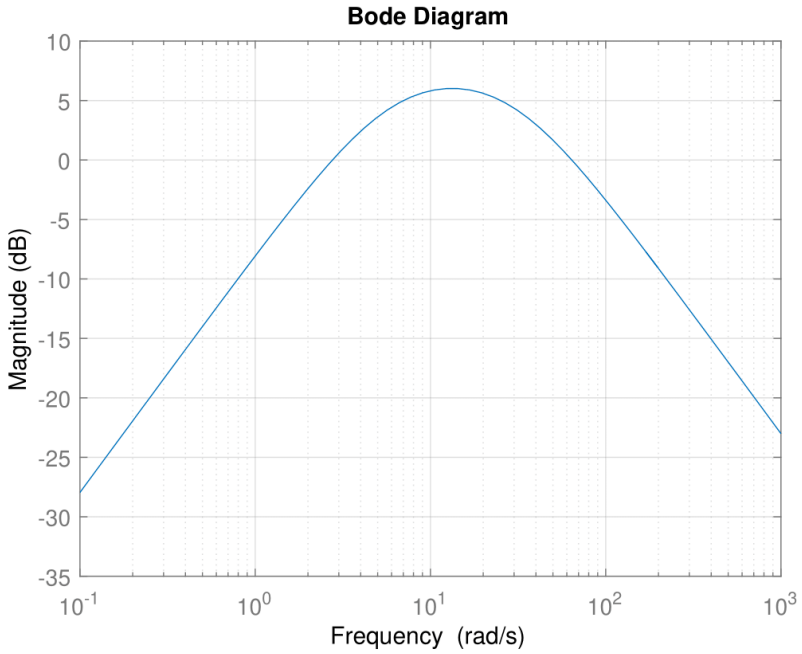

(**a**) NMP portion shown as multiplicative uncertainty bound

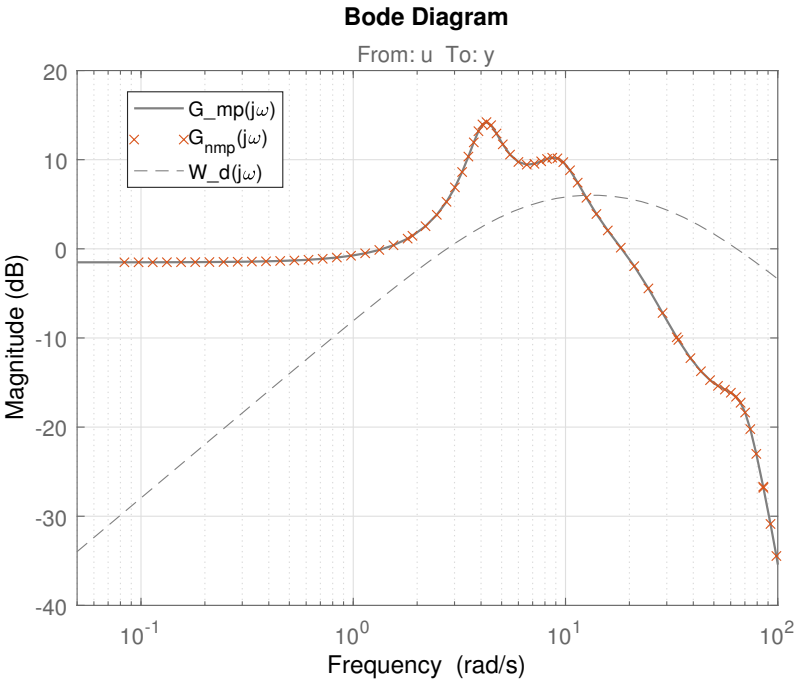

(**b**) Design models and uncertainty bound

Figure 6. Consideration of model factorization.

3. Robust Control Design

The tuning of weighting functions in the H_∞ mixed-sensitivity controller in the optimization process was implemented using *f*mincon() in MATLAB.

The optimized minimization problem by imposing ride quality degradation as a constraint is given by

$$\begin{aligned} \underset{W1\,W2}{\text{minimize}} \quad & f(x) = P_{CT}\,standing \\ \text{subject to} \quad & < \textbf{constraint} = \textbf{rqd} \leq 7.5\% > \end{aligned} \tag{16}$$

The design problem regarding obtaining a model-based controller $K_infty(s)$ is presented in Figure 7. This presented framework is designed to meet several control requirements, such as closed loop stability, a good tracking or disturbance rejection performance, and robust stability in the presence of modeling uncertainties in the model. Here, H_∞ mixed sensitivity was applied on both NMP plant transfer function (G_p) and the MP factorized transfer function (G_{mp}), which is different to what was addressed in [21]. The multiplicative uncertainty bound for the complementary sensitivity, T, has already been obtained for the G_{mp} case.

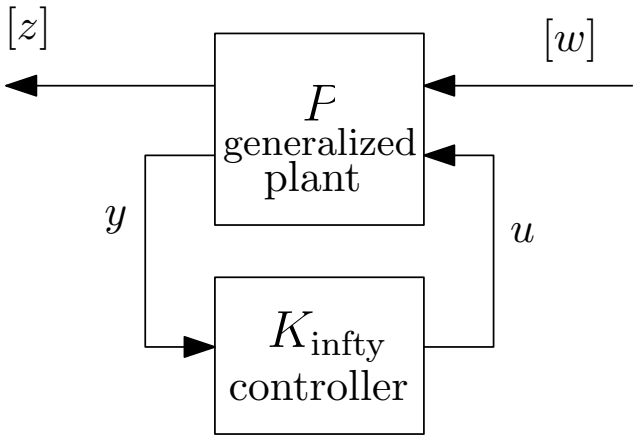

Figure 7. Generalized regulator setup for the H_∞ mixed-sensitivity design.

The nonlinear optimization via different weighted choices is presented in Tables 3 and 4. For P_{2_xNMP} and P_{2_xMP} cases in Table 4, only W1 is obtained via optimization while W_2 and W_3 are fixed. W_3 is W_δ for the NMP (nominal plant G_p) model case and $W_{\delta MP}$ for the MP (factorized plant (G_{mp})) model.

The sensitivity frequency weight, W_1, in Equation (17)'s second-order transfer function formula was introduced by [26]. W_B* represents the maximum frequency bandwidth, M is the maximum peak of sensitivity ($S(j\omega)$), and A is the maximum steady-state tracking error.

The initial value for W_1 parameters was obtained from the PID design in [15]. The upper and lower bound W_1 parameter value for both the NMP and MP model was chosen to be a decade above and lower for optimization purposes.

$$W_1 = \frac{(s/(M^(1/2)) + W_B*)^2}{(s + W_B * (A)^(1/2))^2} \tag{17}$$

The expected range of W_2 in all cases (initial values and fixed level values) was obtained via previous work in [15]. Four (4) cases with different values of fixed W_2 and W_3 for both P_{x2NMP} and P_{x2MP} are presented in Table 4. The values of W_2 used here are 0.75, 0.5, 0.1, and a high-pass filter, respectively, and W_3 is W_δ. Keep in mind that W_2 was used as a high-pass filter introduced here for completeness following the work by [21].

Table 3. Minimization approach identifiers and weight sensitivity parameters (transfer function) for H_∞ mixed-sensitivity optimization (note: rqd denotes ride quality degradation).

Minimization ID	W_1	W_2	W_3
P_{1NMP}	$\frac{s^2+1.317s+0.4337}{1.255s^2+0.06102s+0.0007416}$	0.9355	not used
P_{2NMP}	$\frac{s^2+3.06s+2.341}{2s^2+0.1374s+0.00236}$	0.7047	W_δ
P_{1MP}	$\frac{s^2+0.8792s+0.1932}{1.311s^2+0.03184s+0.0001933}$	0.5338	not used
P_{2MP}	$\frac{s^2+1.063s+0.2823}{2s^2+0.06721s+0.0005646}$	0.309	$W_{\delta MP}$

Table 4. Minimization approach identifiers and weight sensitivity parameters (transfer function) for H_∞ mixed-sensitivity optimization for P_{x2NMP} and P_{x2MP} with fixed W_2 and W_3 (note: rqd denotes ride quality degradation).

$W2_{NMP}$	$W1_{NMP}$	$W2_{MP}$	$W1_{MP}$
W2 = 0.75	$\frac{s^2+3.033s+2.3}{2s^2+0.1356s+0.0023}$	W2 = 0.5	$\frac{s^2+0.972s+0.2362}{1.2s^2+0.03367s+0.0002362}$
W2 = 0.5	$\frac{s^2+2.579s+1.663}{1.972s^2+0.1145s+0.001663}$	W2 = 0.1	$\frac{s^2+1.4s+0.4899}{1.813s^2+0.08429s+0.0009799}$
W2 = 0.1	$\frac{s^2+0.818s+0.1673}{2s^2+0.0413s+0.000213}$	W2 = 0.05	$\frac{s^2+1.407s+0.4949}{1.851s^2+0.08562s+0.0009898}$
$W2_{hpf}$	$\frac{s^2+2.219s+1.231}{1.212s^2+0.09887s+0.002016}$		

4. Nominal Performance Analysis

The full-order H_∞ mixed-sensitivity controller performance on the nominal model for P_{1NMP}, P_{2NMP}, P_{1MP}, and P_{2MP} is presented in Table 5. The table clearly demonstrates how the design is progressing and how the conservatism induced by taking the MP plant into consideration, together with the related uncertainty, affects the design. In fact, the results for the NMP plant are significantly better than the previous analysis presented in [21]. Time-domain lateral acceleration plot responses can be seen in Figure 8. The conservatism of the MP model designed as compare with NMP model can also be proven in the frequency plot in Figures 9–12.

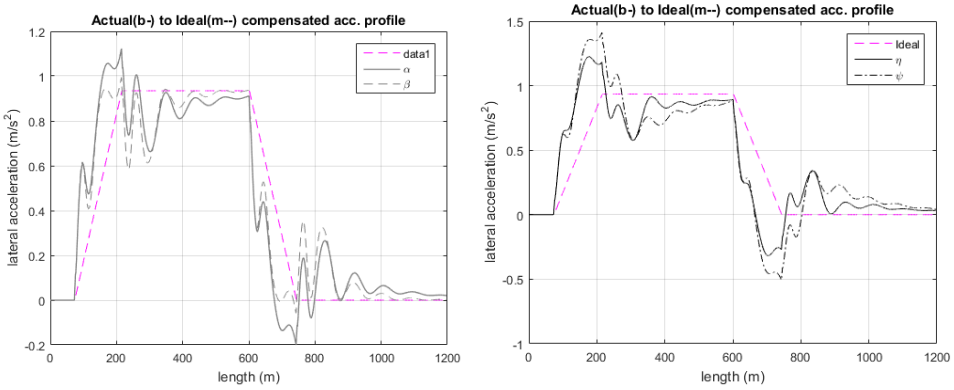

(**a**) (**b**)

Figure 8. Lateral acceleration plot for P_{1NMP}-(α) and P_{2NMP} (β) (**a**), P_{1MP}(η) and P_{2MP} (ψ) (**b**).

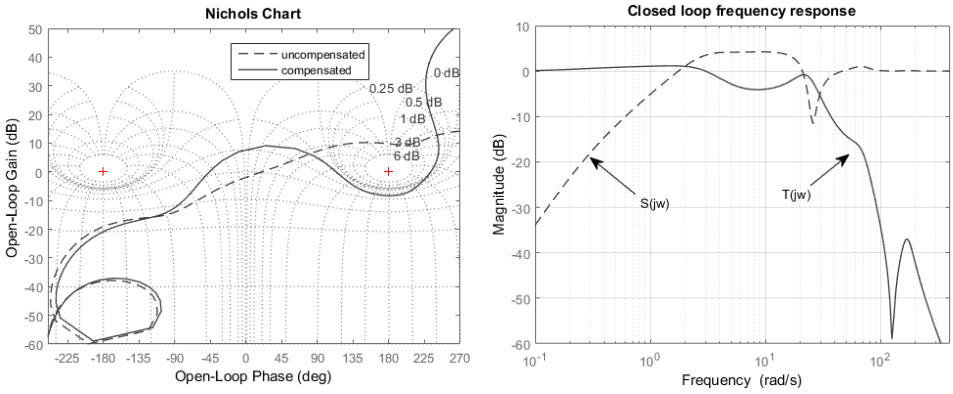

(**a**) (**b**)

Figure 9. Open loop (**a**) and closed loop (**b**) complementary sensitivity ($T(j\omega)$) and sensitivity ($S(j\omega)$) plots for P_{1NMP} case.

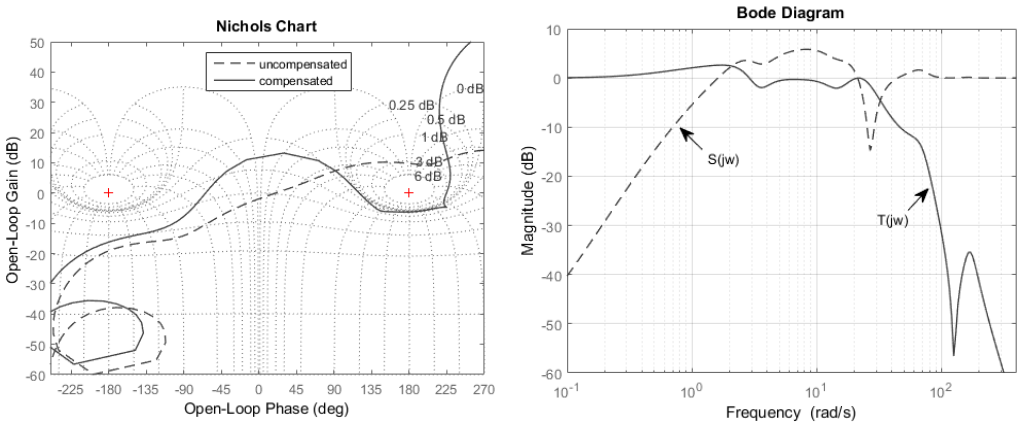

(**a**) (**b**)

Figure 10. Open loop (**a**) and closed loop (**b**) complementary sensitivity ($T(j\omega)$) and sensitivity ($S(j\omega)$) plots for P_{2NMP} case.

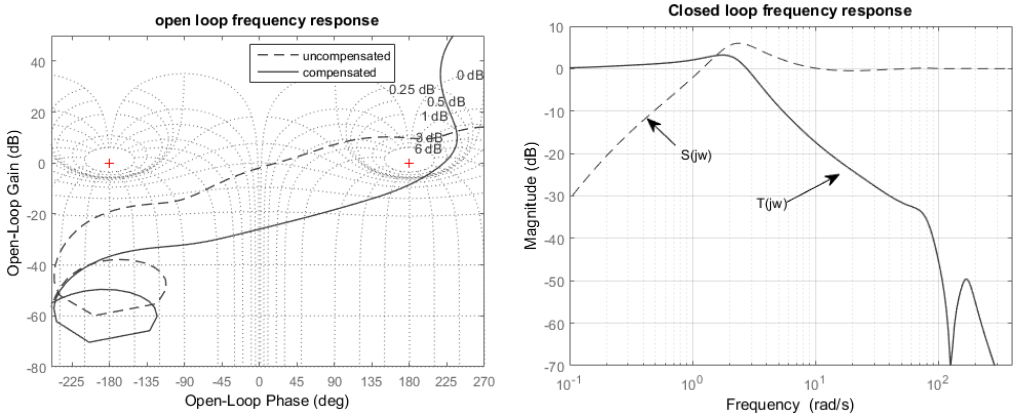

(**a**) (**b**)

Figure 11. Open loop (**a**) and closed loop (**b**) complementary sensitivity ($T(j\omega)$) and sensitivity($S(j\omega)$) plots for P_{1MP} case.

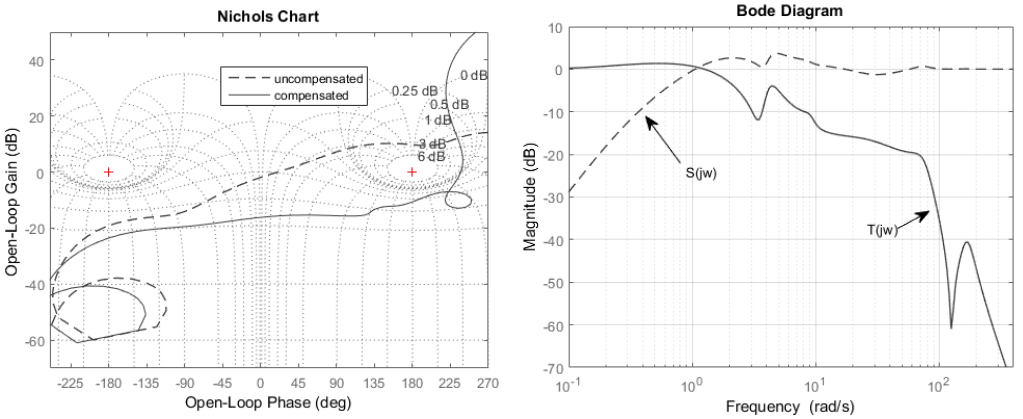

(**a**) (**b**)

Figure 12. Open loop (**a**) and closed loop (**b**) complementary sensitivity ($T(j\omega)$) and sensitivity ($S(j\omega)$) plots for P_{2MP} case.

Tables 6 and 7 show the result for the nominal performance of P_{x2NMP} (NMP case) and P_{x2MP} (MP case), respectively. A value of ride quality trade-off below 7.5 can be achieved with W_2 values of 0.75 and 0.5. The controller design with MP cases, however, shows a much higher P_{CT} performance resulting from imposing extra conservativeness on the MP model. This is proven from the sensitivity plot shown in Figure 13 for the P_{x2NMP} $W_2 = 0.5$

and P_{x2MP} $W_2 = 0.1$ case. P_{x2MP} $W_2 = 0.1$ shows a very narrow gap between $S(jw)$ and γ/W_1 in Figure 13.

Table 5. H_∞ Mixed-sensitivity controller performance assessment with the different time-domain optimization approaches.

Deterministic (as Per Given Units)		P_{1NMP}	P_{2NMP}	P_{1MP}	P_{2MP}
Lateral accel.	RMS deviation (%g)	2.194	2.064	2.921	3.474
	Peak value (%g)	11.434	10.137	12.476	14.388
Roll gyro.	RMS deviation (rad/s)	0.024	0.024	0.031	0.033
	Peak value (rad/s)	0.118	0.124	0.127	0.114
	Peak jerk level (%g/s)	6.495	6.279	8.025	7.933
P_{CT}-related	Standing (% of passenger)	48.703	46.41	57.359	58.672
	Seated (% of passenger)	13.029	11.912	15.737	16.832
Stochastic (acceleration %g) @58 m/s [1]					
Ride quality	Tilting train	3.059	3.052	3.063	2.914
	Degradation (%)	7.413	7.166	7.55	2.331
Performance Margins					
Freq. resp.	Gain margin (dB)	8.306	6.243	8.475	10.607
	Phase margin (deg)	52.682	44.513	41.083	57.123
	Bandwidth (rad/s)	1.25	1.23	0.809	0.723
	$\|S(j\omega)\|_\infty$	1.625	1.952	1.993	1.535
	Gamma γ	1.3139	1.3221	0.8409	0.6412

[1] Ride quality for non-tilting train if running at the higher speed = 2.848%g.

The tilt performance for fixed W_2 for the remaining system identifiers P_{x2NMP}, P_{x2MP} is presented in Tables 6 and 7. The proposed robust design for this case shows that the best result is obtained from the NMP case, though the MP case gives a consistent tilt performance.

Table 6. H_∞ Mixed-sensitivity controller performance assessment with the different fixed W_2 values for P_{x2NMP} case.

Deterministic (as per Given Units)		W_2 **0.75**	W_2 **0.5**	W_2 **0.1**	W_2 **HPF**
P_{CT}-related	Peak jerk level (% g/s)	6.29	6.674	9.004	7.140
	Standing (% of passenger)	46.341	48.706	66.045	52.106
	Seated (% of passenger)	11.902	12.786	20.138	14.124
Stochastic (acceleration %g) @58 m/s [1]					
Ride quality	Tilting train	3.056	3.032	3.062	2.957
	Degradation (%)	7.306	6.462	7.52	3.840
Performance Margins					
Freq. resp.	Gain margin (dB)	6.142	7.484	15.858	8.540
	Phase margin (deg)	44.19	48.263	65.457	52.718
	$\|S(j\omega)\|_\infty$	1.974	1.736	1.195	1.596
	Gamma γ	1.294	1.112	0.623	1.446

[1] Ride quality for non-tilting train if running at the higher speed = 2.848%g.

From the control theoretical point of view, if the γ values obtained are larger than 1, the desired specification in the stacked requirements is not precisely realized. However, it is not a crucial point in this case since the controller design in the optimization process presented

in this paper prioritized the tilt control performance rather than just the obtained value of γ. For completeness, sensitivity plots with respect to γ/W_1 are illustrated in Figure 13.

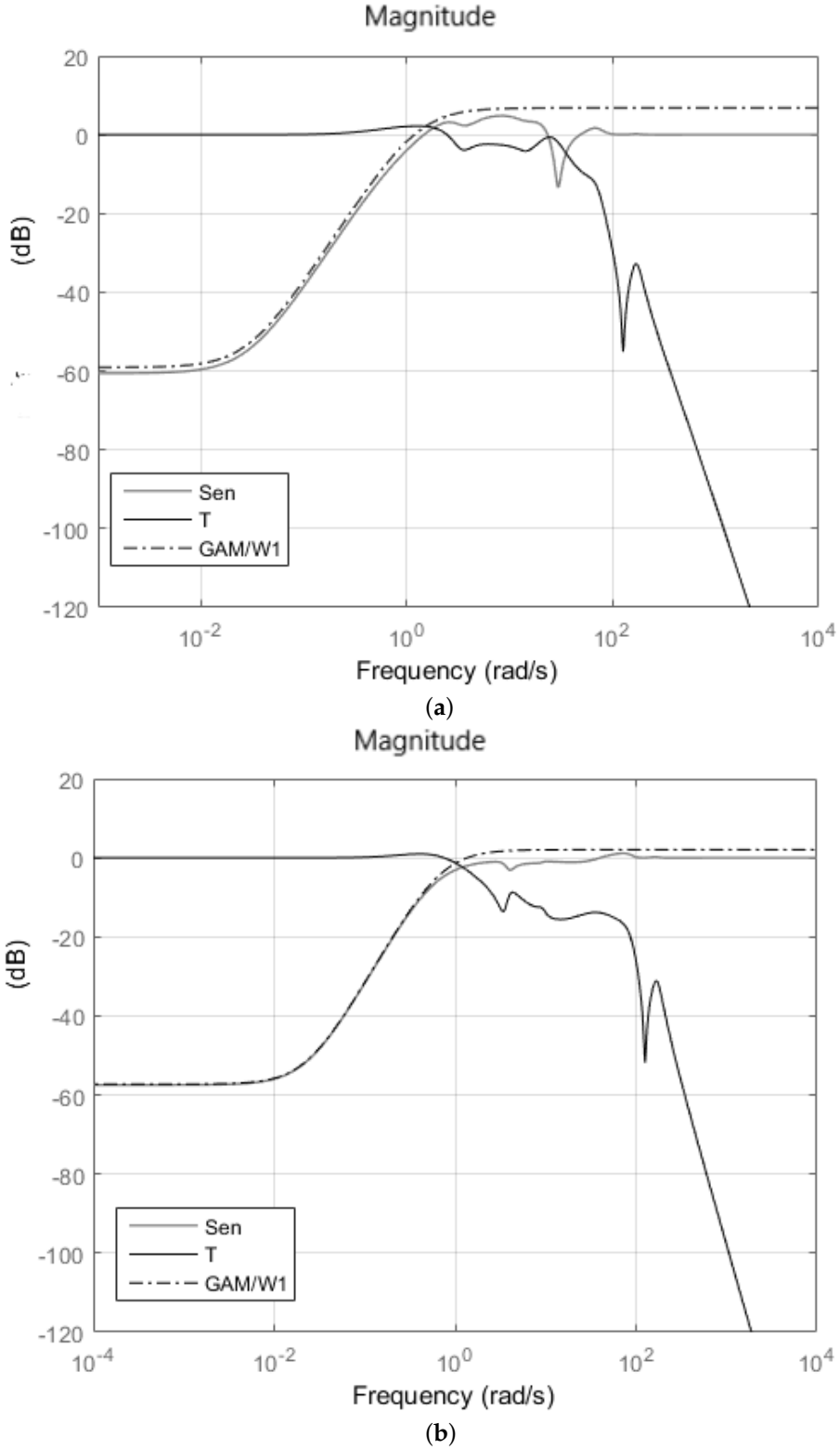

Figure 13. Sensitivity (S), complementary sensitivity (T), and γ/W_1 plot for (**a**) $P_{x2NMP}\,W_2 = 0.5$; (**b**) $P_{x2MP}\,W_2 = 0.1$.

Table 7. H_∞ Mixed-sensitivity controller performance assessment with the different fixed W_2 values for P_{x2MP} case.

Deterministic (as per Given Units)		W_2 **0.5**	W_2 **0.1**	W_2 **0.05**
P_{CT}-related	Peak jerk level (% g/s)	7.647	7.638	7.671
	Standing (% of passenger)	56.884	56.451	56.595
	Seated (% of passenger)	15.964	15.897	15.973
Stochastic (acceleration %g) @58 m/s [1]				
Ride quality	Tilting train	3.062	2.961	3.022
	Degradation (%)	7.497	3.971	6.120
Performance Margins				
Freq. resp.	Gain margin (dB)	8.689	10.299	10.508
	Phase margin (deg)	55.339	55.307	55.538
	$\|S(j\omega)\|_\infty$	1.827	1.585	1.559
	Gamma γ	0.9130	0.6869	0.6752

[1] Ride quality for non-tilting train if running at the higher speed = 2.848%g.

Controller Reduction and Robust Performance Investigation

Since the H_∞ controllers used here were model-based, the controller order achieved from the optimization design tended to be large (can be up to 18th order in this case and differs for each case). Following the same controller reduction method as that presented in [15], we briefly provide controller reduction results here. It can be concluded from Figure 14 that the P_{CT} and ride quality performance trade-off are still maintained up to a seventh-order reduction for all cases.

The controller must meet both nominal and robust stability requirements in order to guarantee the robustness of the system's performance. Note that, in order to achieve the control specifications, one should strictly talk about performance rather than just stability—though here we only refer to bounds for stability. We offer a straightforward method for expressing multiplicative uncertainty as the parametric uncertainty on the actual design transfer function (including NMP zeros). While the case in the previous Section 4 was easily obtained analytically, here, the bound was obtained in the form of an envelope covering a wide range of frequency responses.

Here, four choices of plant perturbation, including nominal plant $P0$, were used for robust performance analysis, i.e., refer to Table 2.

We offer a succinct discussion on robust performance based on the reduced controllers that were produced. The reduced controller order used for robust performance analysis here was the eighth order based on the analysis performed in Figure 14. In addition, note that only six (6) "best" cases are presented here.

The results of the eighth-reduced-order controller on the robust tilt performance of for all six cases are given in Tables 8 and 9. It can be said that, for all chosen cases, the P_{CT} factor performance is maintained for all four (4) plant uncertainty cases of $P1$, $P2$, $P3$, and $P4$. The worst ride quality degradation is maintained below 15% for all three MP models (P_{1MP}, P_{2MP}, and P_{2xMP}) on the $P1$, $P2$, and $P3$ plant due to the extra conservativeness of the MP model. However, the MP model P_{1MP} cannot maintain a below 15% worst ride quality degradation performance for the $P4$ uncertainty plant. In fact, $P4$ is the worst plant uncertainty case since the NMP model shows an unstable performance on this plant. Although the robustness of more conservative controller designs tends to be better, they may fall short of the expected improvement in nulling-type tilt control performance (which should be as close as possible to the performance provided by a tilt with a precedence equivalent).

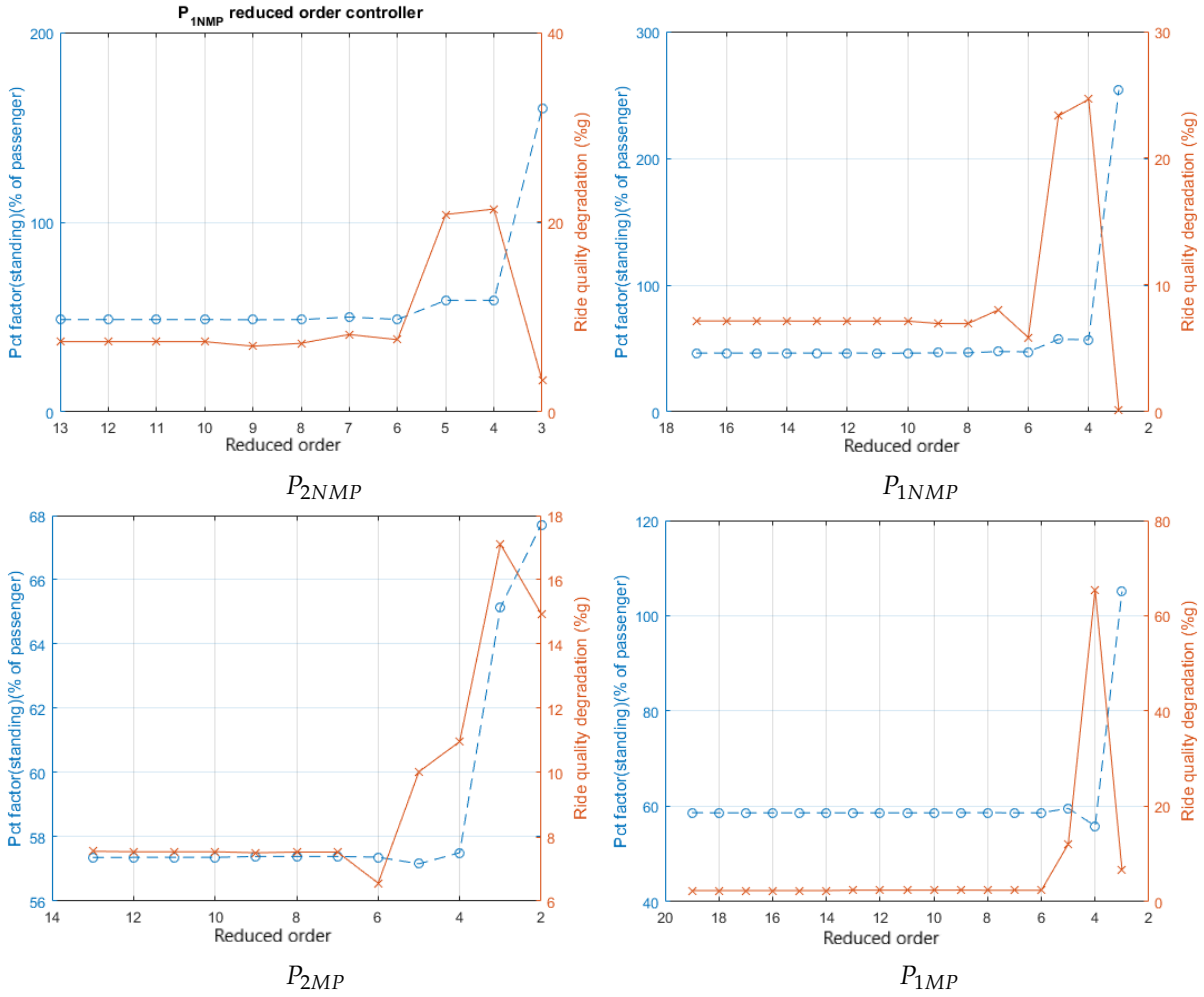

Figure 14. Controller reduction and performance trade-off for H_∞ mixed-sensitivity cases. The blue line represents P_{CT} factor of standing passenger, the red line represents ride quality degradation.

Table 8. Robust performance for P_{CT} standing for 8th-order H_∞ controller.

Case	P0 Nominal	P1	P2	P3	P4
P_{1NMP}	48.674	49.965	50.264	50.606	51.688
P_{2NMP}	46.535	46.196	48.957	57.200	47.904
$P_{2xNMP0.5}$	48.816	49.583	49.910	50.230	50.662
P_{1MP}	57.392	59.567	55.362	55.571	63.388
P_{2MP}	58.682	62.161	59.943	60.860	65.678
$P_{2xMP0.1}$	56.667	59.831	58.944	59.765	63.196

The results obtained (for the nominal models) via this proposed robust controller approach compared to the ones obtained by [21] are much improved (esp. the PCT factor for $P_{2xNMP0.5}$, P_{2NM}, P_{1NMP}; note that the ride quality is a constraint, i.e., should be $\leq$7.5%, and is not the primary concern to optimize: the deterministic response is the primary point to address and optimize). Note that the best PCT obtained in [21] is approx. 51.7%. In addition, the work in this paper studied the robust performance in detail. Similar conclusions can be drawn comparing the results to the ones obtained in [22] (PCT obtained is approx. 62%). A direct comparison is possible as the track excitation input (deterministic, stochastic) is the same in all cases.

Table 9. Robust performance for ride quality for 8th-order H_∞ controller.

Case	P0 Nominal	P1	P2	P3	P4
P_{1NMP}	7.241	29.453	14.539	36.730	unstable
P_{2NMP}	6.966	24.418	22.475	92.808	unstable
$P_{2xNMP0.5}$	6.210	15.509	17.379	35.497	69.424
P_{1MP}	7.527	14.288	4.581	4.168	29.282
P_{2MP}	2.403	5.866	−0.481	−1.253	10.002
$P_{2xMP0.1}$	4.372	7.692	2.698	2.137	13.244

5. Conclusions

This paper rigorously studied optimized H_∞ mixed sensitivity in tilt control design in the context of a single-input–single-output control framework. In particular, the impact of the proposed controller in a nominal and multiplicative uncertainty plant of both an MP and NMP model was presented and compared. The detailed nominal and robust performance of H_∞ mixed sensitivity in both a nominal and multiplicative uncertainty plant was illustrated via simulation results. The robust controller design was followed via a twofold method: (i) using the non-minimum phase design model and (ii) proposing a factorized design model version with the non-minimum phase characteristics treated as uncertainty. Rigorous analysis provided useful insights in selecting the best tilt controller to obtain a trade-off between the nominal performance and robust performance. While this work addressed tilt control design, the proposed approach can be applied to active suspension of a similar nature and other applications exhibiting non-minimum phase characteristics in their representative model.

Author Contributions: Conceptualization, F.H. and A.Z.; writing—original draft, F.H.; formal analysis, F.H.; supervision, A.Z.; validation, F.H.; writing—reviewing and editing, F.H., A.Z. and G.H.; investigation, F.H.; visualization, F.H.; resources, F.H., A.Z. and G.H.; methodology, F.H.; software, F.H. All authors have read and agreed to the published version of the manuscript.

Funding: This research was funded by the Ministry of Education Malaysia under Fundamental Research Grant Scheme (FRGS).

Data Availability Statement: Results can be duplicated directly from data information provided in the article. Data sharing is not applicable to this article.

Acknowledgments: The authors would like to acknowledge the financial support from the Ministry of Education Malaysia under Fundamental Research Grant Scheme(FRGS) FRGS/1/2019/TK08/UTM/02/3.

Conflicts of Interest: The authors declare no conflict of interest.

Abbreviations

The following abbreviations are used in this manuscript:

GPS	Global Positioning System
SISO	Single-Input–Single-Output
NMP	Non-Minimum Phase
MP	Minimum Phase
PID	Proportional Integral Derivative
TF	Transfer Function

Appendix A. Variables and Parameters List

y_v, y_b, y_0	Lateral displacement of body, bogie, and railtrack (m)
$\dot{y}_v, \dot{y}_b, \dot{y}_0$	Roll rate of body, bogie, and railtrack (m/s)
θ_v, θ_b	Roll displacement of body, bogie, and actuator (rad)
$ffi_t, \dot{ffi}_t$	Applied tilt (rad) and tilt rate (rad/s)
$R^{-1}, \dot{R}^{-1}$	Curve radius rate and acceleration
θ_0	Rail track cant, curve radius (rad)
θ_r	Airspring reservoir roll deflection (rad)
v	Vehicle forward speed (tilting: 58 m/s)
m_v	Half body mass, 19,000 (kg)
i_{vr}	Half body inertia, 25,000 (kgm)
m_b	Bogie mass, 2500 (kg)
i_{br}	Bogie roll inertia, 1500 (kgm^2)
k_{az}	Airspring area stiffness, 210×10^3 N/m
k_{sz}	Airspring series stiffness, 620×10^3 N/m
k_{rz}	Airspring reservoir stiffness, 244×10^3 N/m
c_{rz}	Airspring reservoir damping, 33×10^3 Ns/m
k_{sy}	Secondary lateral stiffness, 260×10^3 N/m
c_{sy}	Secondary lateral damping, 33×10^3 Ns/m
$y_w, \dot{y}_w$	Bogie kinematics position (m), rate (m/s)

References

1. Iwnicki, S. *Handbook of Railway Vehicle Dynamics*; CRC Press: Boca Raton, FL, USA, 2006.
2. Vickerman, R. High-speed rail in Europe: Experience and issues for future development. *Ann. Reg. Sci.* **1997**, *31*, 21–38. [CrossRef]
3. Fröidh, O. Perspectives for a future high-speed train in the Swedish domestic travel market. *J. Transp. Geogr.* **2008**, *16*, 268–277. [CrossRef]
4. Darlton, A.O.; Marinov, M. Suitability of tilting technology to the tyne and wear metro system. *Urban Rail Transit* **2015**, *1*, 47–68. [CrossRef]
5. Stribersky, A.; Steidl, S.; Müller, H.; Rath, B. On dynamic analyses of rail vehicles with electronically controlled suspensions. *Veh. Syst. Dyn.* **1996**, *25*, 614–628. [CrossRef]
6. Pearson, J.T.; Goodall, R.M.; Pratt, I. Control system studies of an active anti-roll bar tilt system for railway vehicles. *Proc. Inst. Mech. Eng. Part J. Rail Rapid Transit* **1998**, *212*, 43–60. [CrossRef]
7. Huber, B.H. The bogie-based tilt option-simplicity and flexibility. *Proc. Inst. Mech. Eng. Part J. Rail Rapid Transit* **1998**, *212*, 19–32. [CrossRef]
8. Persson, R.; Goodall, R.M.; Sasaki, K. Carbody tilting–technologies and benefits. *Veh. Syst. Dyn.* **2009**, *47*,949–981. [CrossRef]
9. Zolotas, A.; Goodall, R.M.; Halikias, G.D. New control strategies for tilting trains. *Veh. Syst. Dyn.* **2002**, *37*, 171–182. [CrossRef]
10. Bruni, S.; Goodall, R.; Mei, T.X.; Tsunashima, H. Control and monitoring for railway vehicle dynamics. *Veh. Syst. Dyn.* **2007**, *45*, 743–779. [CrossRef]
11. Hohenbichler, N.; Six, K.; Abel, D. The Benefit of Skyhook control in high speed railway vehicles. *Ifac Proc. Vol.* **2006**, *39*, 890–895. [CrossRef]
12. Zhao, Y.; Wang, T.; Karimi H.R. Distributed cruise control of high-speed trains. *J. Frankl. Inst.* **2017**, *354*, 6044–6061. [CrossRef]
13. Ye, J.; Sun, H. The Influence of an Integration Time Step on Dynamic Calculation of a Vehicle-Track-Bridge under High-Speed Railway. *Math. Digit. Publ. Inst.* **2021**, *9*, 431. [CrossRef]
14. Zamzuri, H.; Zolotas, A.C.; Goodall, R.M. Tilt control design for high-speed trains: A study on multi-objective tuning approaches. *Veh. Syst. Dyn.* **2008**, *46*, 535–547. [CrossRef]
15. Hassan, F.; Zolotas, A.C.; Margetts, R. Improved PID control for tilting trains. In Proceedings of the 2016 IEEE International Conference for Students on Applied Engineering (ICSAE), Newcastle Upon Tyne, UK, 20–21 October 2016.
16. Hassan, F.; Zolotas, A. Impact of fractional order methods on optimized tilt control for rail vehicles. *Fract. Calc. Appl. Anal.* **2017**, *20*, 765–789. [CrossRef]
17. Chaudhuri, B.; Pal, B.C.; Zolotas, A.C.; Jaimoukha, I.M.; Green, T.C. Mixed-sensitivity approach to $H\infty$ control of power system oscillations employing multiple FACTS devices. *IEEE Trans. Power Syst.* **2003**, *18*, 1149–1156. [CrossRef]
18. Fales, R.; Kelkar, A. Robust control design for a wheel loader using mixed sensitivity H-infinity and feedback linearization based methods. In Proceedings of the 2005, American Control Conference, Portland, OR, USA, 8–10 June 2005; pp. 4381–4386.
19. Bakouri, M.; Alassaf, A.; Alshareef, K.; Abdelsalam, S.; Ismail, H.F.; Ganoun, A.; Alomari, A.-H. An Optimal H-Infinity Controller for Left Ventricular Assist Devices Based on a Starling-like Controller: A Simulation Study. *Mathematics* **2022**, *10*, 731. [CrossRef]

20. Yan, S.-R.; Alattas, K.A.; Bakouri, M.; Alanazi, A.K.; Mohammadzadeh, A.; Mobayen, S.; Zhilenkov, A.; Guo, W. Generalized Type-2 Fuzzy Control for Type-I Diabetes: Analytical Robust System. *Mathematics* **2022**, *10*, 690. [CrossRef]
21. Zolotas, A.C. Advanced Control Strategies for Tilting Trains. Ph.D. Thesis, Loughborough University, Loughborough, UK, 2002.
22. Zolotas, A.C.; Wang, J.; Goodall, R.M. Reduced-order robust tilt control design for high-speed railway vehicles. *Veh. Syst. Dyn.* **2008**, *46*, 995–1011. [CrossRef]
23. Zolotas, A.C.; Goodall, R.M. Advanced control strategies for tilting railway vehicles. In *UKACC International Conference on Control*; University of Cambridge: Cambridge, UK, 2000.
24. Al-Baidhani, H.; Sahib, A.; Kazimierczuk, M.K. State Feedback with Integral Control Circuit Design of DC-DC Buck-Boost Converter. *Mathematics* **2023**, *11*, 2139. [CrossRef]
25. Ivanov, D.; Granichin, O.; Pankov, V.; Volkovich, Z. Design of $\ell 1$ New Suboptimal Fractional Delays Controller for Discrete Non-Minimum Phase System under Unknown-but-Bounded Disturbance. *Mathematics* **2022**, *10*, 69. [CrossRef]
26. Skogestad, S.; Postlethwaite, I. *Multivariable Feedback Control: Analysis and Design*; Wiley: Hoboken, NJ, USA, 2007; Volume 2.

Disclaimer/Publisher's Note: The statements, opinions and data contained in all publications are solely those of the individual author(s) and contributor(s) and not of MDPI and/or the editor(s). MDPI and/or the editor(s) disclaim responsibility for any injury to people or property resulting from any ideas, methods, instructions or products referred to in the content.

https://dspace.org/

New insights on robust control of tilting trains with combined uncertainty and performance constraints

Hassan, Fazilah; Zolotas, Argyrios; Halikias, George

2023-07-02
MDPI
https://doi.org/10.3390/math11143057
Hassan F, Zolotas A, Halikias G. (2023) New insights on robust control of tilting trains with combined uncertainty and performance constraints. Mathematics, Volume 11, Issue 14, July 2023, Article number 3057

Downloaded from a DSpace repository. https://dspace.org/